Chinese Chemical Letters 31 (2020) 792–796

Contents lists available at ScienceDirect

Chinese Chemical Letters

journal homepage: www.elsevier.com/locate/cclet

Communication

Nitrogen photofixation on holey g-C_3N_4 nanosheets with carbon vacancies under visible-light irradiation

Jianhua Ge[a,b,*], Long Zhang[a], Jing Xu[a], Yujie Liu[a], Daochuan Jiang[b], Pingwu Du[b,*]

[a] School of Earth and Environment, Anhui University of Science & Technology, Huainan 232001, China
[b] CAS Key Laboratory of Materials for Energy Conversion, Department of Materials Science and Engineering, Collaborative Innovation Center of Chemistry for Energy Materials (iChEM), University of Science and Technology of China (USTC), Hefei 230026, China

ARTICLE INFO

Article history:
Received 15 April 2019
Received in revised form 10 May 2019
Accepted 13 May 2019
Available online 18 May 2019

Keywords:
Nitrogen photofixation
Carbon vacancies
g-C_3N_4
Nanosheets
Photocatalysis

ABSTRACT

Nitrogen photofixation using g-C_3N_4-based photocatalysts have attracted abundant of attentions recently. Herein, in this study, holey g-C_3N_4 (HGCN) nanosheets possess a good deal of carbon vacancies were prepared by means of thermally treating bulk g-C_3N_4 (BGCN) under an NH_3 atmosphere. Characterization analysis revealed that the as-synthesized sample have identical crystal structure, larger BET specific surface area, stronger reduction capability, and higher photogenerated charge carrier separation rate than that of BGCN. These properties may contribute to enhance the nitrogen photofixation activity. It was also found that the rate of NH_4^+ production for N_2 photofixation of HGCN sample reached ~25.54 mg L^{-1} h^{-1} g^{-1}_{cat}, which is approximately ~5.87 times higher than that of BGCN sample under optimal reactive conditions. Moreover, a plausible mechanism of HGCN for nitrogen photofixation process was illuminated in detail.

As we all known, nitrogen is an essential element of organism in the process of metabolism. Although, nitrogen gas account for about 78% of the atmosphere, in view of its intrinsically strong nonpolar covalent triple bond of N≡N, nitrogen gas molecular is difficult to utilize directly by most of organism on earth [1–4]. Along with the development of the global economy, the biological nitrogen fixation only rely on bacteria is difficult to satisfy the increased demand of modern industry and agriculture [5,6]. Meanwhile, the traditional Haber-Bosch nitrogen fixation process under high pressure and temperature, which would release large amounts of carbon dioxide into the atmosphere, and accelerate the greenhouse effect [7,8]. Therefore, over the past few decades, teams of researchers have been studying the green nitrogen fixation process under mild reaction conditions [9,10].

In the recently, photocatalysis technique have been widely deemed as an ideal process to replace the Haber-Bosch nitrogen fixation industrial processes with an improved photocatalyst, owing to its green, gentle reaction conditions, low energy consumption, and so on [11–13].

As early as in 1977, Schnauzer and his coworkers first covered that N_2 molecules can be reduced to ammonia using Fe-doped rutile TiO_2 *via* UV-light irradiation [14]. Since then, plenty of novel nitrogen photofixation systems have been developed successively, for instance, metal oxide-based materials systems, metal sulfide-based materials systems, bismuth oxyhalides systems, carbonaceous materials systems, and other potential materials systems, and so forth [12,15–19].

It is well known that Wang and collaborators for the first time reported a novel metal-free photocatalyst g-C_3N_4 in 2009 [20]. Since then, a mass of literatures have been published on the aspect of g-C_3N_4 materials for nitrogen photofixation. However, the nitrogen fixation performance of g-C_3N_4 is severely hampered due to the absence of photocatalytic active centers and rapid migration rate of photoexcited electrons-holes of bulk g-C_3N_4 [21]. Massive efforts have been devoted by scientific researchers to settle those bottlenecks [22–24]. Among those strategies, one modification is to establish hetero structure junction with another conductive materials to improve the separation efficiency of photo-excited electron-hole of photocatalyst [21,25–27]. The other way is to construct porous structure with large specific surface area of g-C_3N_4, which could expose more chemical active centers and chemical adsorption sites for photocatalytic activity [28]. Besides the above summarizations, in present studies, most researchers have been extensively focused on fabricating vacancy (mainly

* Corresponding authors at: CAS Key Laboratory of Materials for Energy Conversion, Department of Materials Science and Engineering, Collaborative Innovation Center of Chemistry for Energy Materials (iChEM), University of Science and Technology of China (USTC), Hefei 230026, China.
E-mail addresses: jhge@aust.edu.cn (J. Ge), dupingwu@ustc.edu.cn (P. Du).

https://doi.org/10.1016/j.cclet.2019.05.030
1001-8417/

including oxygen vacancies, sulfur vacancies, and nitrogen vacancies) in the different photocatalysts systems, which is inspired by the successful nitrogen photofixation *via* oxygen vacancies on the surface of BiOBr nanosheets under visible-light irradiation [16,19]. For instance, Yang's research group fabricated in-plane holey g-C_3N_4 nanosheets containing carbon vacancies by thermal ammonolysis of bulk g-C_3N_4, which has a dramatic higher photocatalytic H_2 evolution rate of nearly 20 folds higher than that of bulk g-C_3N_4 [29].

Excited by the above generalization, we hypothesize that carbon vacancies formed by the thermal ammonolysis of bulk g-C_3N_4, not only act as chemical active sites to activate nitrogen molecules but also promote photo-excited electron-holes separation, due to O, N and S atom have the similar chemical properties. The bulk g-C_3N_4 was thermally treated by means of ammonization method, and investigated in detail for nitrogen photofixation, which exhibits significantly enhanced performance under visible light. Characterization results indicated that the as-synthesized sample have identical crystal structure, larger BET specific surface area, stronger reduction capability, and higher photogenerated charge carrier separation rate, which could be attributed to the nitrogen photofixation ability. Furthermore, the nitrogen photofixation mechanism using HGCN under visible light was discussed.

All the chemical reagents (analytical grade), mainly including melamine ($C_3H_6N_6$, >98.0% purity), ethylene glycol ($C_2H_6O_2$, >98% purity), sodium sulfite (Na_2SO_3, >99%), Nessler's reagent (>99.5% purity) and triethanolamine ($C_6H_8O_6$, >98% purity), were purchased from Aldrich or Aladdin and received without further purification.

The bulk g-C_3N_4 was synthesized based on our group's reported method [30,31]. Melamine powder (~2.5 g) was directly heated at 550 °C for 240 min at a rate of 2.5 °C/min in the muffle furnace. After milling, the obtained yellow powder was denoted as BGCN.

The holey g-C_3N_4 was obtained according to calcine the above bulkg-C_3N_4 powders (~0.3 g) were calcined at 510 °C for 60 min at a rate of 5 °C/min under NH_3 gas atmosphere, and denoted as HGCN. For comparison, bulk g-C_3N_4 (~0.3 g) was calcined at 510 °C for 60 min under air atmosphere, and denoted as AGCN.

All the obtained photocatalysts were systematically performed using XRD (D/max-TRIII, 5°/min, 10°~70° in 2θ, Japan) equipment, FT-IR (BrukerT27, Germany), SEM (FEI, Sirion-200, equipped with an electron diffraction, Holland), BET(ASAP2020, Micromeritics, USA), photoluminescence (Edinburgh FLS-920, Britain), X-ray photoelectron spectroscopy (XPS, ESCA-Lab 250, USA) and UV–vis spectrometer (Solid-3700, Japan).

The nitrogen photofixation reactions were carried out in a ~250 mL double-walled quartz flask, 300 W Xe lamp (Perfect Light Co., Ltd.) as the irradiation source, about 0.2 g of the photocatalyst was dispersed in ~200 mL of aqueous solution containing hole trapping agents, and the NH_4^+ production were quantified utilizing the Nessler's reagent spectrophotometry standard curve method.

In order to acquire information about the crystal structure of BGCN, HGCN and AGCN, the as-prepared samples were examined using powder X-ray diffraction, and the characterization analysis results were displayed in Fig. S1 (Supporting information). The two characteristic diffraction peaks at 13.1° and 27.4° of the samples are ascribed to (100) and (002) of crystal plane of g-C_3N_4, which are distinct evidence of the periodic in-plane tri-*s*-triazine motif units and interlayer melon aromatic packing, respectively. Interesting, compare with BGCN, the intensity of the (002) decreased, and the near absence of the (100) peak HGCN and AGCN reveal that a few-layered morphology structure nanosheets of HGCN are formed [32–34]. Meanwhile, the (002) peak of HGCN skews to a higher angle, demonstrating interaction between the g-C_3N_4 layers and NH_3. Furthermore, the HGCN sample display similar XRD pattern with HGCN, and AGCN, indicated that the overall crystal structure of HGCN was not changed by the mean of ammonization method modification [29].

With aim to understand the surface morphology of photocatalyst samples, SEM and TEM measurements were further investigated (Fig. 1). As illustrated in Fig. 1a, the BGCN sample reveals the typical stacked lamellar morphology structure. After treated at 510 °C under air atmosphere, the surface of AGCN has been partial corroded (Fig. 1b), and promote exfoliation of BGCN, resulting in reducing the dimensions of the sample (Fig. 1e). At same time, etching BGCN using NH_3 gas at 510 °C in tube furnace, the HGCN are highly corrugated, and the holey structure with abundant in-plane holes in HGCN are formed (Fig. 1c). The TEM analysis results further confirm that the HGCN are laminar and contain abundant nanopores (Fig. 1f).

The nitrogen adsorption-desorption isotherms together with the corresponding pore size distribution were further use to analysis porous structure of the HGCN, AGCN and BGCN. As shown in Fig. S2 (Supporting information), all the samples exhibite the

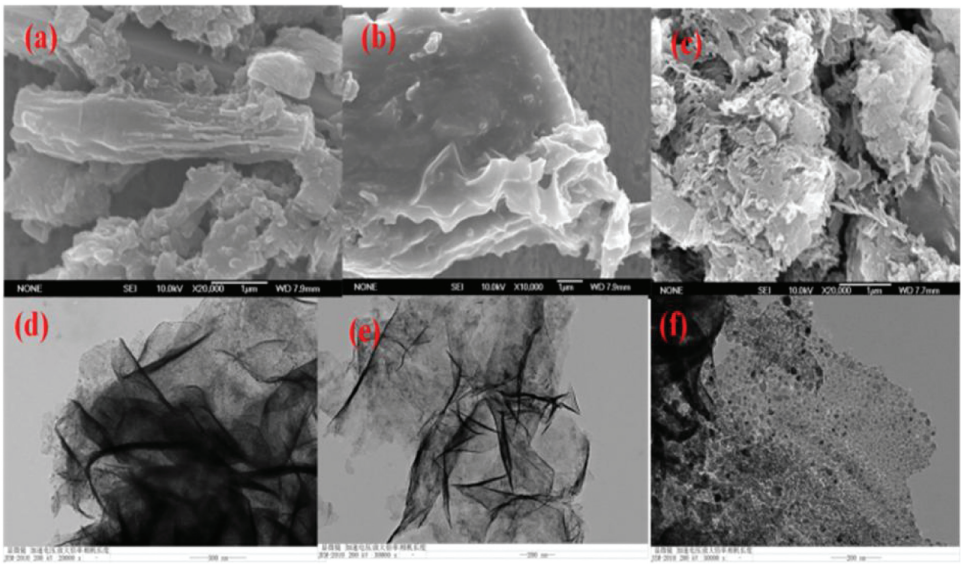

Fig. 1. The surface morphologies of samples: SEM of BGCN (a), AGCN (b) and HGCN (c); TEM of BGCN (d), AGCN (e) and HGCN (f).

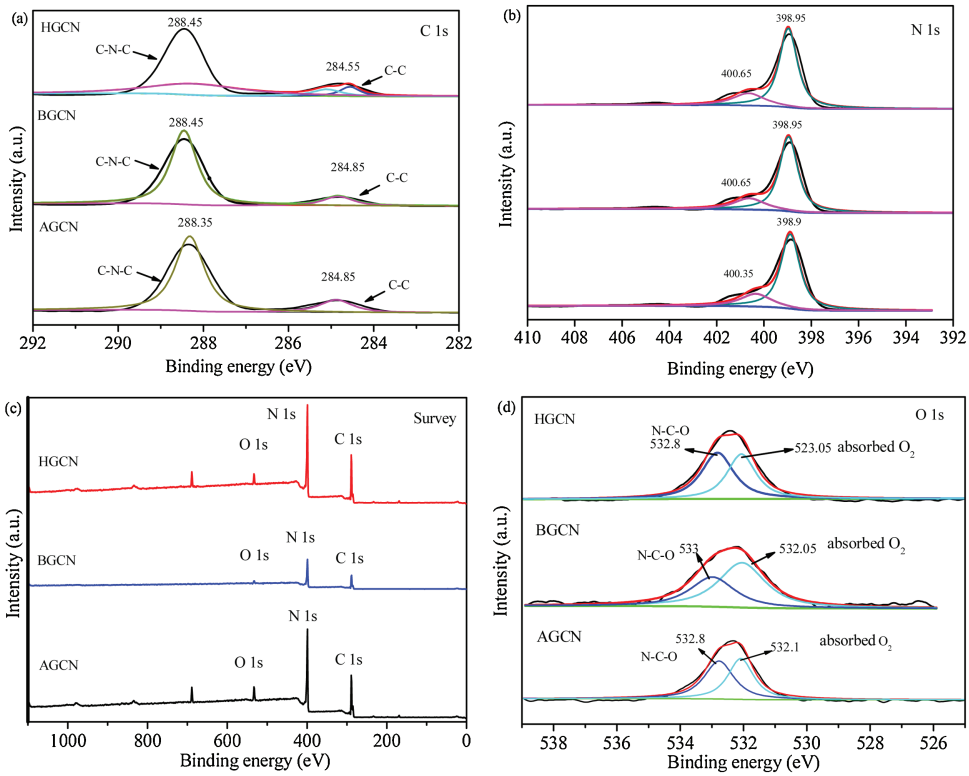

Fig. 2. (a) XPS survey spectra and high-resolution XPS spectra: C 1s (b), N 1s (c) and Ni 2p (d) of the samples.

typical H3-type hysteresis loop according to the IUPAC classification, indicating the presence of mesopores [35,36]. Clearly, after thermal ammonization method treatment, the BET specific surface area of HGCN sample is calculated to be ~33.86 m^2/g, which is almost 6 times larger than that of BGCN (~5.65 m^2/g). Moreover, using Barret-Joyner-Halender (BJH) method, the pore size of the HGCN is calculated from density functional theory analysis to be around 20 nm is smaller than the pore size of the AGCN and BGCN sample. Compared with AGCN, BGCN sample reveal an increase in BET surface areas and decrease in pore size which may be caused by the NH_3 etching, and the nanoporous framework may benefiting the nitrogen photofixation process.

As shown in Fig. S3 (Supporting information), the FT–IR spectra of HGCN, BGCN, and BGCN exhibited identical characteristic peaks at ~810 cm^{-1}, and ~1200-1600 cm^{-1}, which are ascribed to the typical stretching modes of C—N heterocycles and the bending vibration of heptazine rings, indicating all the as-synthesized samples are made up of heptazine units, and have the similar chemical structure. Noticeable, the characteristic peaks of HGCN are sharper than those of BGCN due to the more ordered packing of tri-s-triazine motifs in the g-C_3N_4 nanosheets [37].

The optical properties of the as-prepared HGCN, BGCN, and BGCN were investigated by UV–vis measurement. It can be clearly found that all three samples possess visible-light absorbance. Compared with BGCN, the absorption edge of HGCN is blue-shifted from ~475 nm to ~425 nm. Furthermore, a broader and stronger absorption tail phenomenon, starting at ~550 nm and extending to the near-infrared region (800~1400 nm), is also clearly observed (Fig. S4a in Supporting information), may be caused by the presence of carbon vacancies. Meanwhile, the bandgap of HGCN, AGCN, and BGCN is calculated to be ~2.95 eV, ~2.90 eV, ~2.80 eV, respectively using the Kubelka-Munk function, may owning to the effect of quantum confinement effect in the structure of HGCN nanosheets. Compare with BGCN, the photo-excited electrons on HGCN have stronger the thermodynamic reduction capability [38].

With aim to analyze the chemical states and surface composition of the as-synthesized HGCN, AGCN, and BGCN specimens using XPS measurement. As shown in Fig. 2, the survey scan XPS spectrum of all the samples clearly displays the existence of C, N, and O elements. It should be noted that the C element serve as the reference, and O element might be from the absorbed H_2O, O_2, and CO_2 molecules. Meanwhile, the high-resolution XPS spectra reveal that there is no obvious variation in the binding energy of C 1s, N 1s and O 1s, manifesting that the chemical state and structure of the HGCN, AGCN, and BGCN are almost the same [39,40]. Moreover, the obtained C/N mass ratio of HGCN, BGCN and AGCN were *ca.* ~0.4969, ~0.5412, and ~0.5258 according to the XPS analysis respectively, which is less than the theoretic value of the g-C_3N_4 (~0.5625), suggesting the carbon vacancies are obtained treating AGCN under air atmosphere (Table S1 in Supporting information).

PL spectra analysis is often used to characterize the migration and recombination process of photo-excited electron-hole pairs in photocatalyst samples. Lower PL spectrum intensity suggested more photo-excited charge carriers were migrated or trapped [30]. As shown in Fig. S5a (Supporting information), the as-prepared samples possess the similar emission peak at ~440 nm, which is assigned to the recombination of photo-excited charge carriers in g-C_3N_4. Meanwhile, the PL spectra intensity of HGCN decreased compared with AGCN and BGCN, demonstrating that the recombination extent of photo-generated charge carriers was inhibited more significantly in HGCN, which would contribute to improve the nitrogen photofixation activity.

The transient photocurrent response curves of the photoelectrodes decorated with AGCN, BGCN, and HGCN samples were recorded using CHI660 electrochemical workshop in 0.5 mol/L Na_2SO_4 aqueous solution. As shown in Fig. S5b (Supporting information), all of working electrode decorated with sample present scarcely any photocurrents without visible-light irradiation. When the Xenon lamp turn on, an obviously enhanced photocurrent curve appears. The interesting phenomenon can be

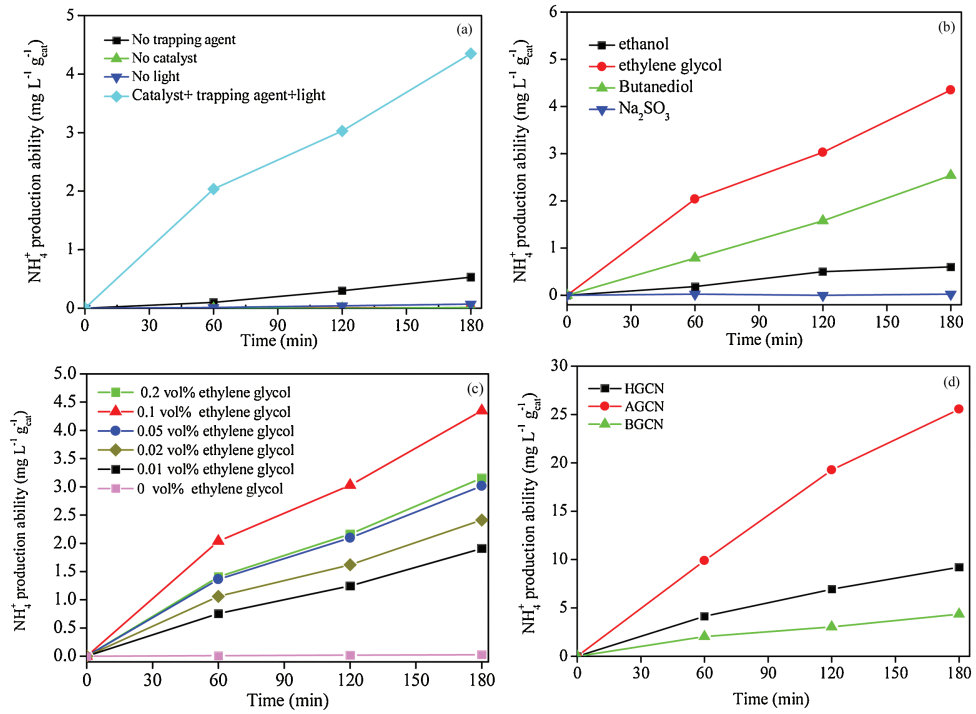

Fig. 3. The N_2 photofixation activity of the samples.

ascribed to the migration of the photo-excited charge carriers under visible-light irradiation. Meanwhile, the working electrode decorated with HGCN sample displays enhanced photo-current than that of the AGCN and BGCN sample, due to the surface of HGCN has more carbon vacancies and higher BET specific surface areas which was beneficial to improve the photo-excited charge carriers' migration from the interface of the photocatalyst to the adsorbed N_2.

The nitrogen photofixation experiments were performed in aqueous solution using AGCN, HGCN, and BGCN under visible light irradiation. As seen in Fig. 3a, the concentration of NH_4^+ production ability is almost zero without the photocatalyst or no light irradiation, with addition of trapping agent in above N_2 photofixation system, the NH_4^+ production ability increased. When photocatalyst, trapping agent and visible light were employed together, the NH_4^+ production ability increased sharply. The effect of the type and volume concentration of trapping agent for the N_2 photofixation were further investigated using photocatalyst samples BGCN. As Figs. 3b and c illustrated, compared with the ethanol, Na_2SO_3 and butanediol, the ethylene glycol electron donors together with 0.1% ethylene glycol can enhance the nitrogen photofixation activity sharply. Furthermore, the rate of NH_4^+ production for N_2 photofixation of HGCN reached ~25.54 mg L^{-1} h^{-1} g^{-1}_{cat}, which is approximately ~5.87 times higher than that of BGCN under optimal reactive conditions (Fig. 3d).

On basis of the above experimental analysis, a plausible mechanism of HGCN for nitrogen photofixation process is proposed and illuminated in Scheme 1. When HGCN photocatalyst was illuminated under visible-light, the photo-electrons in VB will be excited to the CB of HGCN sample. Furthermore, carbon vacancies in HGCN with plentiful localized electrons can strengthen adsorption of inert N_2 gas molecules and indirectly activated to N_2^* according to form adsorption geometry. Meanwhile, surface carbon vacancies in HGCN possess their typical defect state can restrain charge carries recombination, and may able to promote the photo-generated electrons to the transiently charged electronic states of N_2^* [38]. Moreover, the transiently charged electronic

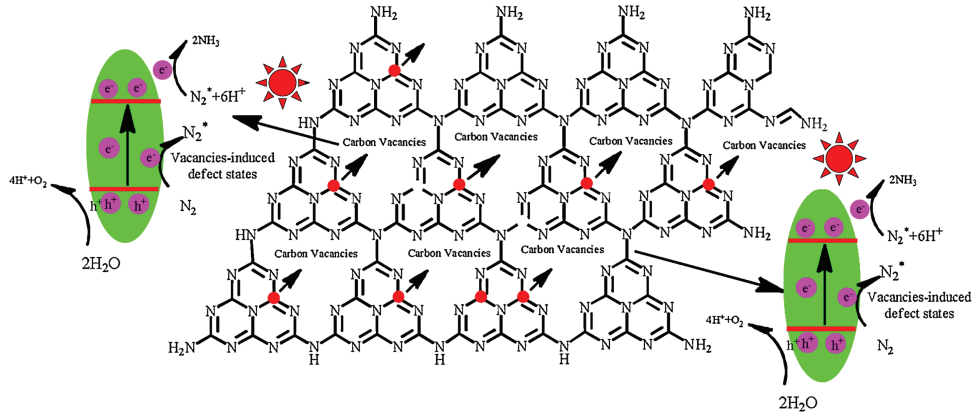

Scheme 1. Mechanism of nitrogen photofixation using HGCN.

states of N_2^* can dramatically lower the energy barrier for the interfacial charge transfer for nitrogen photofixation reactions. Thus, compared with BGCN and AGCN samples, the efficiently improved nitrogen photofixation activity of HGCN could be allied to the following reasons: (1) The expanding specific area could induce more reactive sites; (2) The carbon vacancies in HGCN sheets not only contribute to adsorb and activate N_2 molecules, but also facilitate photo-excited charge separation rate. (3) The expanded band gap of HGCN resulting in the photo-excited electrons possesses enhanced reduction potential for nitrogen photofixation [38].

In summary, HGCN nanosheets possess a good deal of carbon vacancies were achieved by means of thermally treating BGCN under an NH_3 atmosphere. Compare with BGCN and AGCN, the as-synthesized HGCN sample has identical crystal structure, larger BET specific surface area, stronger reduction capability, and higher photogenerated charge carrier separation rate, which may contribute to enhance the nitrogen photofixation activity. It was also drew the conclusion that the rate of NH_4^+ production for N_2 photofixation of HGCN sample reached $\sim$25.54 mg L^{-1} h^{-1} g^{-1}_{cat}, which is approximately $\sim$5.87 times higher than that of BGCN sample under optimal reactive conditions. Finally, a plausible mechanism of HGCN for nitrogen photofixation process was illuminated.

Acknowledgments

We acknowledge the National Key Research and Development Program of China (No. 2017YFA0402800), the National Natural Science Foundation of China (Nos. 51772285, 21473170 and 51878004), and the Natural Science Fund of Anhui Province (No. 1808085ME139) for partly funded support.

Appendix A. Supplementary data

Supplementary material related to this article can be found, in the online version, at doi:https://doi.org/10.1016/j.cclet.2019.05.030.

References

[1] M. Li, H. Huang, J. Low, et al., Small Methods (2018) 1800388.
[2] Q. Liu, L. Ai, J. Jiang, J. Mater. Chem. A 6 (2018) 4102–4110.
[3] Y. Zhao, Y. Zhao, G.I.N. Waterhouse, et al., Adv. Mater. 29 (2017) 1703828.
[4] C. Ling, X. Niu, Q. Li, A. Du, J. Wang, J. Am. Chem. Soc. 140 (2018) 14161–14168.
[5] X. Chen, N. Li, Z. Kong, W.J. Ong, X. Zhao, Mater. Horiz. 5 (2018) 9–27.
[6] K. Hoshino, Chem. -Eur. J. 7 (2001) 2727–2731.
[7] S. Wang, X. Hai, X. Ding, et al., Adv. Mater. 29 (2017) 1701774.
[8] W. Zhao, J. Zhang, X. Zhu, et al., Appl. Catal. B. Environ. 144 (2014) 468–477.
[9] X. Li, X. Sun, L. Zhang, S. Sun, W. Wang, J. Mater. Chem. A 6 (2018) 3005–3011.
[10] J. Li, H. Li, G. Zhan, L. Zhang, Acc. Chem. Res. 50 (2017) 112–121.
[11] Y.H. Cao, Y.F. Tong, J. Zhang, et al., Chem. J. Chin. Univ.-Chin. 37 (2016) 1357–1363.
[12] S. Hu, X. Chen, Q. Li, Y. Zhao, W. Mao, Catal. Sci. Technol. 6 (2016) 5884–5890.
[13] Y. Wang, Y. Yu, R. Jia, C. Zhang, B. Zhang, Natl. Sci. Rev. 4 (2019) 730–738.
[14] G.N. Schrauzer, T.D. Guth, J. Am. Chem. Soc. 99 (1977) 7189–7193.
[15] Y. Cao, S. Hu, F. Li, et al., RSC Adv. 6 (2016) 49862–49867.
[16] S. Hu, Y. Li, F. Li, et al., ACS Sustain. Chem. Eng. 4 (2016) 2269–2278.
[17] K. Hoshino, M. Inui, T. Kitamura, H. Kokado, Angew. Chem. Int. Ed. 39 (2000) 2509–2512.
[18] G. Dong, W. Ho, C. Wang, J. Mater. Chem. A 3 (2015) 23435–23441.
[19] H. Li, J. Shang, Z.H. Ai, L.Z. Zhang, J. Am. Chem. Soc. 137 (2015) 6393–6399.
[20] X. Wang, K. Maeda, A. Thomas, et al., Nat. Mater. 8 (2008) 76–78.
[21] W.J. Ong, L.K. Putri, L.L. Tan, et al., Appl. Catal. B Environ. 180 (2016) 530–543.
[22] B. Li, L. Shao, B. Zhang, et al., J. Colloid. Interface Sci. 505 (2017) 653–663.
[23] K.H. Liu, H.X. Zhong, S.J. Li, et al., Prog. Mater. Sci. 92 (2018) 64–111.
[24] N. Meng, J. Ren, Y. Liu, et al., Energy Environ. Sci. 11 (2018) 566–571.
[25] X. She, J. Wu, H. Xu, et al., Adv. Energy Mater. 7 (2017) 1700025.
[26] B. Zeng, L. Zhang, X. Wan, H. Song, Y. Lv, Sens. Actuator. B -Chem. 211 (2015) 370–376.
[27] X. Dong, F. Cheng, J. Mater. Chem. A 3 (2015) 23642–23652.
[28] J.W. Fu, J.G. Yu, C.J. Jiang, B. Cheng, Adv. Energy Mater. 8 (2018) 1701503.
[29] Q. Liang, Z. Li, Z.H. Huang, F. Kang, Q.H. Yang, Adv. Funct. Mater. 25 (2015) 6885–6892.
[30] J. Ge, Y. Liu, D. Jiang, L. Zhang, P. Du, Chin. J. Catal. 40 (2019) 160–167.
[31] J. Ge, D. Jiang, L. Zhang, P. Du, Catal. Lett. 148 (2018) 3741–3749.
[32] Y. Deng, L. Tang, G. Zeng, et al., Appl. Catal. B: Environ. 203 (2017) 343–354.
[33] Z.L. Ni, F. Dong, H.W. Huang, Y.X. Zhang, Catal. Sci. Technol. 6 (2016) 6448–6458.
[34] S. Zhao, Y. Zhang, Y. Zhou, et al., Carbon 126 (2018) 247–256.
[35] L.Q. Yang, J.F. Huang, L. Shi, et al., Appl. Catal. B: Environ. 204 (2017) 335–345.
[36] J. Ge, X. Guo, X. Xu, et al., RSC Adv. 5 (2015) 49598–49605.
[37] X.H. Li, X. Wang, M. Antonietti, Chem. Sci. 3 (2012) 2170–2174.
[38] Y. Cui, J. Zhang, G. Zhang, et al., J. Mater. Chem. 21 (2011) 13032–13039.
[39] T. Xiao, Z. Tang, Y. Yang, et al., Appl. Catal. B: Environ. 220 (2018) 417–428.
[40] H. Dong, X. Guo, C. Yang, Z. Ouyang, Appl. Catal. B: Environ. 230 (2018) 65–76.